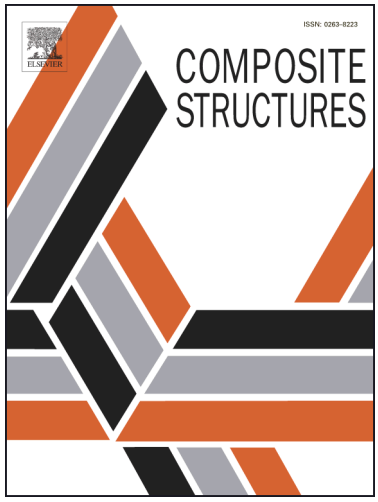

Dynamic instability of variable angle tow composite plates with delamination

Xiaodong Chen, Guojun Nie, Zhangming Wu

PII: S0263-8223(17)33167-7
DOI: https://doi.org/10.1016/j.compstruct.2017.12.042
Reference: COST 9199

To appear in: *Composite Structures*

Received Date: 26 September 2017
Revised Date: 20 November 2017
Accepted Date: 15 December 2017

Please cite this article as: Chen, X., Nie, G., Wu, Z., Dynamic instability of variable angle tow composite plates with delamination, *Composite Structures* (2017), doi: https://doi.org/10.1016/j.compstruct.2017.12.042

Dynamic instability of variable angle tow composite plates with delamination

Xiaodong Chen [a]; Guojun Nie [a]; Zhangming Wu [b,a*]

[a] School of Aerospace Engineering and Applied Mechanics, Tongji University, 1239 Siping Road, Shanghai 200092, China

[b] Cardiff School of Engineering, Queens Buildings, The Parade, Newport Road, Cardiff CF24 3AA, UK

Corresponding Author: Zhangming Wu* **E-mail: wuz12@cardiff.ac.uk z.wu@tongji.edu.cn**

Guojun Nie* **E-mail: ngj@tongji.edu.cn**

Abstract: In this paper, the dynamic instability of variable angle tow (VAT) plates with a single rectangular delamination is studied using an analytical model. The analytical model is derived from the principle of potential energy based on the classical laminated plate theory. Both global and local behavior of delaminated VAT plates in the dynamic instability analysis are accurately captured by the use of multiple Legendre polynomial series. The equations for the motion in dynamic instability problem are derived using Hamilton's principle. The dynamic instability regions are determined from the resulting Mathieu differential equations, which are solved using Bolotin's approach. To validate the proposed analytical model, both critical buckling loads and natural frequencies of delaminated VAT plates are evaluated and compared with FEM results. The influence of delamination on the buckling load, natural frequency and dynamic instability region (DIR) of delaminated VAT plates is examined by numerical examples. A parametric study is subsequently carried out to analyze the effect of linearly varying fibre orientation angles on the dynamic instability response of delaminated VAT plates. Finally, the mechanism of applying variable angle tows to improve the dynamic stability performance of delaminated composite plates is studied.

Keywords: Dynamic instability; Variable angle tow composites; Laminated plates; Rayleigh-Ritz method; Delamination

1 Introduction

Thin-walled structures like plates and shells that are used as primary components in aviation, automotive and civil industry are often subjected not only to static loads but also to dynamic loads. Structures under time-dependent (i.e. periodic) in-plane loads might lead to unacceptable vibration at a critical combination of excitation frequency and the amplitude of the axial load, namely *parametric resonance*. Understanding the characteristics of *parametric resonance* of composite structures under a dynamic loading is also of importance in practical designs. The advantages of applying variable angle tow (VAT) laminates that generally possess variable stiffness properties to

improve structural performance have been clearly shown in previous works, in terms of buckling [1-5], postbuckling [6, 7] and vibration [8, 9]. However, dynamic stability problem of VAT composite structures subjected to in-plane periodic loads has received little attention in variable stiffness composites research community. Delamination caused by the impact of foreign objects (tool drops, runway debris, bird strikes etc) or manufacturing process, is one of the most common damage forms in composite laminates. The existence of delamination between plies reduces the structural stiffness, strength and load-carrying capacity, and thus may give rise to early instability or failure to composite structures. This paper presents an analytical study of dynamic instability performance of VAT composite plates with a rectangular delamination. The mechanism of varying fiber orientation angles (VAT) resulting in the improved dynamic stability of composite plates with delamination is thoroughly investigated.

A considerable amount of research has been done on the dynamic instability analysis of composite laminated plates without delamination. Bolotin [10] initially studied the dynamic instability of various elastic systems under periodic in-plane loadings. Afterwards, Birman [11] studied the dynamic instability of unsymmetrically laminated cross-ply plates under periodic biaxial loading. In his work, the principal dynamic instability region was determined analytically. Srinivasan and Chellapandi [12] used the finite strip method (FSM) based on classical laminated plate theory to perform the dynamic instability analysis for composite laminated plates under periodic in-plane load. Moorthy et al. [13] and Chattopadhyay and Radu [14] carried out a similar investigation using the finite element method based on the first-order and higher-order shear deformation theories to approximate the instability regions for moderately thick composite plates. In addition, Mond and Cederbaum [15] used the method of multiple scales to carry out the dynamic instability analysis of antisymmetric angle-ply and cross-ply laminated plates. Wang and Dawe [16] investigated the dynamic instability of composite laminated plate and prismatic plate structures. Sahu and Datta [17] performed the dynamic instability analysis of composite laminated plates subjected to non-uniform harmonically varying in-plane loading. Recently, Samukham et al. [18] investigated the dynamic instability of a VAT composite plate under periodic in-plane compressive loading using the finite element method. In their work, considerable benefits from steered fibers in improving the dynamic stability behavior of VAT composite plates without delaminations were demonstrated.

There also has been a significant amount of research on the dynamic response of composite laminated beam-plates or plates with delamination. Wang et al. [19] initially proposed the free model to perform the free vibration analysis for isotropic beam-plates with a through-the-width delamination by considering the coupling between flexural and axial vibrations of delaminated sublaminates. However, vibrational mode shapes obtained using the free model may be physically inadmissible for an off-midplane delamination. To address this problem, Mujumdar and Suryanarayan [20] developed a constrained model, in contrast to the free model proposed by Wang et al. [19], to study the natural vibration characteristics of laminated beam type structures. In their

work, delaminated portions were constrained to have identical transverse deformations. Later, Shen and Grady [21] conducted an analytical and experimental investigation for the vibration response of a cantilever beam-plate with a through-the-width delamination. Lee [22] studied the vibration characteristics of delaminated beam-plates using finite element method based on the layerwise plate theory. Luo and Hanahud [23] developed an analytical model that can consistently explain the phenomena observed by experiments [21], to predict frequencies of delaminated beam-plates. In addition, Shu and Della [24] applied Euler-Bernoulli beam theory to investigate the free vibration of composite beams with two enveloping delaminations. In their work, both free and constrained models were taken into account in the formulation. Alnefaie [25] developed a three-dimensional finite element model to analyze the dynamic response of fibre-reinforced composite plates with internal delamination. More recently, Li and Qing [26] proposed a nonlinear spring-layer model based on the modified H-R (Hellinger-Reissner) variational principle to perform the free vibration analysis of composite laminated plates with delamination. Liu and Shu [27] adopted Euler-Bernoulli hypothesis to develop an analytical solution for the free vibration of exponential functionally graded beams with a single delamination.

However, there is not much literature available on the dynamic instability response of composite laminated plates, shells or other structures with delamination. Mohanty et al. [28] and Radu and Chattopadhyay [29] used the finite element method based on the first-order and higher-order shear deformation theories, respectively, to investigate the dynamic instability of composite laminated plates with delamination under uniform periodic in-plane loading. Yang and Fu [30] combined Rayleigh–Ritz method with classical shell theory to carry out the dynamic instability analysis for composite laminated cylindrical shells with delamination. Park and Lee [31] applied the higher-order shell theory of Sanders to study the dynamic instability of delaminated spherical shell structures subjected to periodic in-plane loadings. More recently, Noh and Lee [32] investigated the dynamic instability of delaminated composite skew plates under various periodic in-plane loadings. All of the above research works focused on the study of dynamic instability of constant stiffness laminated plates or shells with delaminations. Fazillati [33] recently reported a research work that applied a B-spline finite strip method to study the dynamic instability behavior of variable stiffness composite laminated plates with delamination. However, the non-uniform in-plane stress field was not considered in his model and analysis. A benign non-uniform in-plane stress redistribution given rise by variable stiffness properties had been recognized as the major driver for VAT composite structures to achieve improved performance [1-5] . The characteristics of dynamic instability of delaminated VAT composite plates therefore need to be further clarified.

In the present work, an improved analytical model based on the principle of potential energy and the Rayleigh-Ritz approach was developed to analyze the dynamic instability of VAT composite plates with a single delamination under periodically varying in-plane compressive loadings. In this delamination modelling, both global and local displacement shape functions constructed using the Legendre polynomials are introduced and the kinematic continuity conditions

along the delamination edge are satisfied using the superposition method. The non-uniform in-plane stress distribution is determined prior to the dynamic instability analysis of delaminated VAT plates. The content of this paper is arranged as follows. In the next section, the concept of VAT laminates is introduced. Section 3 presents the basic formulae for the dynamic instability analysis of VAT composite plates with a single delamination, including the constitutive equation, the boundary conditions and the kinematic continuity conditions along the delamination edge. In section 4, the modelling work for solving the in-plane stress and dynamic instability problems of delaminated VAT plates are presented. In section 5, the accuracy and reliability of the proposed analytical model are validated by comparing with numerical results of buckling and vibration of delaminated composite plates with those obtained by FEM and prior results. The influence of delamination on the buckling, vibration and dynamic instability response of delaminated VAT plates is investigated by numerical examples. The mechanism of exploiting variable stiffness properties to improve the dynamic stability of composite laminated plates with a single delamination is also studied in detail. Finally, some conclusions are drawn in Section 6.

2 VAT laminates

The fibre orientation angle of the VAT composite plate varies continuously with spatial location over the entire plane of a ply. In this paper, the fibre orientation angle within a ply is assumed to vary linearly along the length of the plate, given by [34]

$$\theta(x) = \phi + \frac{2(T_1 - T_0)}{a}|x| + T_0 \tag{1}$$

where a is the length of the plate. T_0 is fibre angle at the center of the plate, that is, x=0. And T_1 is fibre angle at the edges of the plate, that is, $x=\pm a/2$. ϕ is the angle of rotation of the fibre path [34]. The fibre orientation angle of a VAT ply is designated by $\phi\langle T_0,T_1\rangle$.

3 Formulation

3.1 Constitutive relation and strain-displacement relation

Consider a VAT composite plate of length a, width b and thickness h, with a single delamination, as shown in Fig. 1. The single delamination is located at mid-length, and the distance from the delamination interface to the top surface is h_1. The VAT composite plate is divided into three portions by the existing delamination interface, namely, an undelaminated portion, denoted by 0, and two delaminated portions, denoted by 1 and 2. The constitutive equations for the L^{th} portion of the delaminated VAT composite plate are given in the following matrix form [35]

$$\begin{Bmatrix} \mathbf{N}^{(L)} \\ \mathbf{M}^{(L)} \end{Bmatrix} = \begin{bmatrix} \mathbf{A}^{(L)} & \mathbf{B}^{(L)} \\ \mathbf{B}^{(L)} & \mathbf{D}^{(L)} \end{bmatrix} \begin{Bmatrix} \boldsymbol{\varepsilon}^{(L)} \\ \boldsymbol{\kappa}^{(L)} \end{Bmatrix} \quad (L = 0,1,2) \tag{2}$$

where $\mathbf{N}^{(L)} = \{N_{xx}^{(L)} \quad N_{yy}^{(L)} \quad N_{xy}^{(L)}\}^{\mathbf{T}}$ and $\mathbf{M}^{(L)} = \{M_{xx}^{(L)} \quad M_{yy}^{(L)} \quad M_{xy}^{(L)}\}^{\mathbf{T}}$, respectively, are the resultant force and bending moment vectors of the L^{th} portion. $\boldsymbol{\varepsilon}^{(L)} = \{\varepsilon_{xx}^{(L)} \quad \varepsilon_{yy}^{(L)} \quad \varepsilon_{xy}^{(L)}\}^{\mathbf{T}}$ and

$\boldsymbol{\kappa}^{(L)} = \{\kappa_{xx}^{(L)} \quad \kappa_{yy}^{(L)} \quad \kappa_{xy}^{(L)}\}^{\mathrm{T}}$, respectively, are the mid-plane strain and curvature vectors of the L^{th} portion. Note that, all these vectors are of time-dependent during the dynamic instability analysis. $\mathbf{A}^{(L)}$, $\mathbf{B}^{(L)}$ and $\mathbf{D}^{(L)}$, respectively, are the in-plane, coupling and bending stiffness matrices of the L^{th} portion and they can be expressed as [35]

$$A_{ij}^{(L)} = \sum_{k=1}^{K^{(L)}} Q_{ij}^{k}\left(z_{k+1} - z_k\right), B_{ij}^{(L)} = \frac{1}{2}\sum_{k=1}^{K^{(L)}} Q_{ij}^{k}\left(z_{k+1}^{2} - z_k^{2}\right), D_{ij}^{(L)} = \frac{1}{3}\sum_{k=1}^{K^{(L)}} Q_{ij}^{k}\left(z_{k+1}^{3} - z_k^{3}\right) \tag{3}$$

where $i, j = 1, 2, 6$ and $K^{(L)}$ is the total number of plies of the L^{th} portion. z_k is the location of the k^{th} ply with respect to the mid-plane of each portion along the thickness direction. Q_{ij}^{k} is the reduced transformed stiffness terms of the k^{th} ply in each portion. For the VAT configuration, Q_{ij}^{k} is functions of the coordinates x and y. Note, the bending-extension coupling within each delaminated portion is taken into account using the method of reduced bending stiffness (RBS) [36], by which the stress resultants are not coupled to the plate curvatures and only related to the curvatures with a reduced stiffness matrix, $\mathbf{D}^{(L)} - [\mathbf{B}^{(L)}]^{\mathrm{T}}[\mathbf{A}^{(L)}]^{-1}[\mathbf{B}^{(L)}]$.

Based on the classical laminated plate theory, the strain-displacement relations of the L^{th} portion in the linear regime can be written as follows [35]

$$\varepsilon_{xx}^{(L)} = \frac{\partial u^{(L)}}{\partial x}, \varepsilon_{yy}^{(L)} = \frac{\partial v^{(L)}}{\partial y}, \varepsilon_{xy}^{(L)} = \frac{\partial u^{(L)}}{\partial y} + \frac{\partial v^{(L)}}{\partial x} \tag{4}$$

$$\kappa_{xx}^{(L)} = -\frac{\partial^2 w^{(L)}}{\partial x^2}, \kappa_{yy}^{(L)} = -\frac{\partial^2 w^{(L)}}{\partial y^2}, \kappa_{xy}^{(L)} = -2\frac{\partial^2 w^{(L)}}{\partial x \partial y} \tag{5}$$

where $u^{(L)}$ and $v^{(L)}$ are the in-plane displacement fields of the L^{th} portion and $w^{(L)}$ the out-of-plane displacement field of the L^{th} portion.

3.2 Boundary conditions and continuity conditions

In this work, delaminated VAT plates loaded by periodically varying uniform axial compression with transverse edges free to deform are taken into account. Hence, the in-plane boundary conditions of the delaminated VAT beam-plate or plate, as shown in Fig. 2 (a) or (b), can be expressed as

$$\bar{N}_{yy} = 0, \bar{N}_{yx} = 0 \qquad \text{at} \quad y = \pm b/2 \tag{6a}$$

$$u^{(0)}(x, y, t) = \mp \bar{u}(t) \qquad \text{at} \quad x = \pm a/2 \tag{6b}$$

where $\bar{N}_{yy}$ and $\bar{N}_{yx}$ are the time-dependent boundary forces on the edges (y=±b/2). $\bar{u}(t)$ is the periodically varying uniform axial compression on the edges (x=±a/2) and expressed in terms of both static and dynamic components, as follows

$$\bar{u}(t) = \bar{u}_{\mathrm{S}} + \bar{u}_{\mathrm{D}}\cos(\Omega t) \tag{7}$$

where $\bar{u}_{\mathrm{S}}$ is the static component of $\bar{u}(t)$; $\bar{u}_{\mathrm{D}}$ is the amplitude of periodically varying dynamic component; Ω is the frequency of external excitation in radian/second. Further, Eq. (7) can be reduced to [18]

$$\overline{u}(t) = \alpha_S u_{cr} + \alpha_D u_{cr} \cos(\Omega t) \tag{8}$$

where u_{cr} is the critical end-shortening value obtained in the buckling analysis. α_S and α_D, are the static and dynamic load parameters, respectively, and defined as,

$$\alpha_S = \frac{\overline{u}_S}{u_{cr}}, \alpha_D = \frac{\overline{u}_D}{u_{cr}} \tag{9}$$

As far as the out-of-plane boundary condition is concerned, there is no limitation to the proposed model presented in this work. The VAT beam-plate with a through-the-width delamination, as shown in Fig. 2(a), is assumed to be simply supported or clamped on the edges (x=±a/2) and free on the edges (y=±b/2), and thus the out-of-plane boundary conditions are given by

$$w^{(0)} = 0 \quad \text{at} \quad x = \pm a/2 \qquad \text{(simply supported)} \tag{10a}$$

$$w^{(0)} = 0; \frac{\partial w^{(0)}}{\partial x} = 0 \quad \text{at} \quad x = \pm a/2 \qquad \text{(clamped)} \tag{10b}$$

The VAT plate with an embedded rectangular delamination, as shown in Fig. 2(b), is assumed to be simply supported or clamped on all four edges. Accordingly, the out-of-plane boundary conditions can be expressed as

$$w^{(0)} = 0 \quad \text{at} \quad x = \pm a/2, y = \pm b/2 \qquad \text{(simply supported)} \tag{11a}$$

$$\begin{aligned} &w^{(0)} = 0; \frac{\partial w^{(0)}}{\partial x} = 0 \quad \text{at } x = \pm a/2 \\ &w^{(0)} = 0; \frac{\partial w^{(0)}}{\partial y} = 0 \quad \text{at } y = \pm b/2 \end{aligned} \qquad \text{(clamped)} \tag{11b}$$

Moreover, the kinematic continuity condition at the intersection of the undelaminated portion and each delaminated portion also needs to be satisfied. In the in-plane stress analysis, the kinematic continuity conditions of the delaminated VAT beam-plate or plate are expressed as

$$\begin{aligned} &u^{(0)} = u^{(L)}, \ \frac{\partial u^{(0)}}{\partial x} = \frac{\partial u^{(L)}}{\partial x}, \ \frac{\partial u^{(0)}}{\partial y} = \frac{\partial u^{(L)}}{\partial y} \\ &v^{(0)} = v^{(L)}, \ \frac{\partial v^{(0)}}{\partial x} = \frac{\partial v^{(L)}}{\partial x}, \ \frac{\partial v^{(0)}}{\partial y} = \frac{\partial v^{(L)}}{\partial y} \end{aligned} \qquad (L = 1, 2) \tag{12}$$

It is noted that the in-plane displacements $u^{(L)}$ and $v^{(L)}$ of the L^{th} delaminated portion on the delamination edge are induced by the translational motion of the undelaminated portion [37]. During the dynamic instability analysis, however, the kinematic continuity conditions at the joint of the undelaminated portion and each delaminated portion are given by

$$\begin{aligned} &w^{(0)} = w^{(L)}, \ \frac{\partial w^{(0)}}{\partial x} = \frac{\partial w^{(L)}}{\partial x}, \ \frac{\partial w^{(0)}}{\partial y} = \frac{\partial w^{(L)}}{\partial y} \\ &u^{(L)} = -z^{(L)} \frac{\partial w^{(0)}}{\partial x}, \ v^{(L)} = -z^{(L)} \frac{\partial w^{(0)}}{\partial y} \end{aligned} \qquad (L = 1, 2) \tag{13}$$

where $z^{(L)}$ is the position of the mid-plane of the L^{th} delaminated portion with respect to the mid-plane of the undelaminated portion along the thickness direction. Different from those in Eq.

(12), the in-plane displacements $u^{(L)}$ and $v^{(L)}$ in Eq. (13) are generated by the rotation of transverse normal of the undelaminated portion along the delamination edge [19, 23, 24, 37-41], as shown in Fig. 3. These in-plane displacements in Eq. (13) eventually lead to the in-plane deformation of the delaminated portions within the delamination region.

4 Solutions

4.1 Non-uniform in-plane stress distribution

VAT composite plates inevitably generate the non-uniform in-plane stress distribution even subjected to a simple axial compression, either displacement-controlled or load-controlled [1, 2, 4]. Accordingly, it is necessary to perform the prebuckling analysis to determine the non-uniform in-plane stress distribution before dynamic instability analysis. For the purpose of simplicity, the following two assumptions are made in prebuckling analysis of delaminated VAT composite plates:

(a) The non-uniform in-plane stress distributions obtained under either static or dynamic in-plane compression loadings are identical [16-18, 32], and therefore the in-plane stress analysis is only performed on delaminated plates loaded by static in-plane compression;

(b) The laminate layup of each portion of the delaminated VAT plate is balanced, as such no extension-shear coupling exists, that is, $A_{16}^{(L)}=0, A_{26}^{(L)}=0$ [35], and therefore only the boundary force $\bar{N}_{xx}$ on the edges (x=±a/2) is necessary to be considered [2, 4, 42].

In the present work, the delaminated VAT plate is subjected to a static uniform axial compression. However, the boundary force distribution $\bar{N}_{xx}$ with respect to a uniform axial compression is implicit and needs to be further determined. Wu and co-workers [2, 42] proposed that the in-plane stress problem of the VAT plate under uniform axial compression can be modelled as a superposition of VAT plates under the action of a series of axial compression loadings, expressed as follows

$$\bar{N}_{xx}(\eta)=\sum_{j=1}^{J}C_jL_j(\eta) \quad \text{at} \quad \xi=\pm 1 \tag{14}$$

where $\eta=2y/b, \xi=2x/a$. C_j is the unknown coefficient of the j^{th} boundary force distribution $L_j(\eta)$ along the edges ($x=\pm a/2$). $L_j(\eta)$ can be represented by the j^{th} Legendre polynomial. The total potential energy Π of the delaminated VAT plate loaded by a uniform axial compression is then expressed as

$$\Pi=\frac{1}{2}\sum_{L=0}^{2}\iint_{\Omega^{(L)}}\left\{\boldsymbol{\varepsilon}^{(L)}\right\}^{\mathrm{T}}[\mathbf{A}^{(L)}]\left\{\boldsymbol{\varepsilon}^{(L)}\right\}\mathrm{d}x\mathrm{d}y-\int_{\Gamma}\bar{N}_{xx}u^{(0)}\mathrm{d}y \tag{15}$$

where $\Omega^{(L)}$ represents the integral area of the L^{th} portion; Γ denotes the boundary edges, that is, $\xi=\pm 1$.

The assumed displacement fields of delaminated VAT plates are expanded in terms of both global and local shape functions, which can be referred to Ref. [43]. Through the minimization of

potential energy in Eq. (15), a set of linear algebraic equations is obtained and expressed in the following matrix form

$$\mathbf{K}^{\mathrm{m}} \cdot \mathbf{U} = \sum_{j=1}^{J} C_j \mathbf{F}_j \tag{16}$$

where $\mathbf{K}^{\mathrm{m}}$ is the membrane stiffness matrix; $\mathbf{U}$ the unknown time-independent coefficient vector; $\mathbf{F}_j$ the vector associated with the j^{th} boundary force $L_j(\eta)$ along the edges ($\xi = \pm 1$). The end-shortening value corresponding to the j^{th} boundary force $L_j(\eta)$ is then evaluated using the following expression [2, 42]

$$\Xi_j(\eta) = u^{(0)}(1,\eta) - u^{(0)}(-1,\eta) \tag{17}$$

Eventually, the unknown coefficients C_j are computed using a least squares method to fit $\Xi_j(\eta)$ with the given uniform end-shortening value Δ [2, 42]. In doing so, the in-plane displacement fields can be obtained by solving the in-plane stress problem in Eq. (16), and then the non-uniform in-plane stress resultants of the delaminated VAT plate loaded by uniform axial compression can be determined from Eq. (2).

4.2 Dynamic instability analysis

In this section, the dynamic instability analysis is performed on the delaminated VAT composite plate under periodically varying uniform axial compression. The strain energy U of the delaminated VAT composite plate is expressed in the following form

$$U = \frac{1}{2}\sum_{L=0}^{2} \iint_{\Omega^{(L)}} \left\{\boldsymbol{\kappa}^{(L)}\right\}^{\mathrm{T}} [\mathbf{D}^{(L)}] \left\{\boldsymbol{\kappa}^{(L)}\right\} \mathrm{d}x\mathrm{d}y + \frac{1}{2}\sum_{L=1}^{2} \iint_{\Omega^{(L)}} \left\{\boldsymbol{\varepsilon}^{(L)}\right\}^{\mathrm{T}} [\mathbf{A}^{(L)}] \left\{\boldsymbol{\varepsilon}^{(L)}\right\} \mathrm{d}x\mathrm{d}y \tag{18}$$

where the second part on the right hand side of Eq. (18) represents the in-plane strain energy stored in each delaminated portions within the delamination region. As mentioned above, the in-plane deformation of each delaminated portion is induced by the rotation of transverse normal of the undelaminated portion along the delamination edge, and thus gives rise to the in-plane strain energy within the delamination region. From the energy point of view, the in-plane strain energy of each delaminated portion can be regarded as a compensation of the bending strain energy reduction of the delamination portions.

The potential energy V of the delaminated VAT composite plate under the action of periodic non-uniform in-plane stress resultants, generated by periodic uniform axial compression, is given by

$$V = \frac{\bar{u}(t)}{2\Delta}\sum_{L=0}^{2} \iint_{\Omega^{(L)}} \left[N_{xx}^{(L)} \left(\frac{\partial w^{(L)}}{\partial x}\right)^2 + N_{yy}^{(L)} \left(\frac{\partial w^{(L)}}{\partial y}\right)^2 + 2N_{xy}^{(L)} \left(\frac{\partial w^{(L)}}{\partial x}\right)\left(\frac{\partial w^{(L)}}{\partial y}\right) \right] \mathrm{d}x\mathrm{d}y \tag{19}$$

The kinetic energy T of the delaminated VAT composite plate during the perturbed motion is expressed as

$$T = \frac{1}{2}\sum_{L=0}^{2} \iint_{\Omega^{(L)}} \rho h^{(L)} \dot{w}^{(L)} \mathrm{d}x\mathrm{d}y \tag{20}$$

where ρ is the mass density and $h^{(L)}$ is the thickness of the L^{th} portion. The over dot of $\dot{w}^{(L)}$ represents differentiation with respect to time.

In this work, the assumed displacement fields are expanded in terms of global shape functions, which satisfy the geometric boundary conditions in Eq. (10) or Eq. (11), as well as local shape functions with null values outside the delamination region. Accordingly, they are expressed as

$$w^{(0)} = W^0_{mn} X^w_m(\xi) Y^w_n(\eta) \tag{21a}$$

$$\begin{aligned} u^{(L)} &= \tilde{U}^L_{pq} \psi^u_{pq}(\xi,\eta) - z^{(L)} W^0_{mn} g_{mn}(\xi,\eta) \\ v^{(L)} &= \tilde{V}^L_{pq} \psi^v_{pq}(\xi,\eta) - z^{(L)} W^0_{mn} h_{mn}(\xi,\eta) \qquad (L=1,2) \\ w^{(L)} &= W^0_{mn} X^w_m(\xi) Y^w_n(\eta) + W^L_{\bar{m}\bar{n}} \psi^w_{\bar{m}\bar{n}}(\xi,\eta) \end{aligned} \tag{21b}$$

where $W^0_{\bar{m}\bar{n}}$, $W^L_{\bar{m}\bar{n}}$, $\tilde{U}^L_{pq}$ and $\tilde{V}^L_{pq}$ (L=1,2) are the time-dependent coefficients relating to $w^{(0)}$, $w^{(L)}$, $u^{(L)}$ and $v^{(L)}$, respectively. The term $X^w_m(\xi)Y^w_n(\eta)$ represents global shape functions, which are constructed by Legendre polynomials multiplying with functions that satisfy the geometric boundary conditions in Eq. (10) or Eq. (11). However, the terms $\psi^u_{pq}(\xi,\eta)$, $\psi^v_{pq}(\xi,\eta)$ and $\psi^w_{\bar{m}\bar{n}}(\xi,\eta)$ represent local shape functions, which are analogous to geometric boundary conditions of clamped edges. The terms $-z^{(L)}W^0_{mn}g_{mn}(\xi,\eta)$ and $-z^{(L)}W^0_{mn}h_{mn}(\xi,\eta)$ are introduced to approximately satisfy kinematic continuity conditions in Eq. (13). For the VAT beam-plate with a through-the-width delamination, both global and local shape functions can be expressed as

$$\begin{aligned} &X^w_m(\xi)Y^w_n(\eta) = (1-\xi^2)L_m(\xi)L_n(\eta) \\ &\psi^w_{\bar{m}\bar{n}}(\xi,\eta) = (\beta_1^2-\xi^2)^2 L_{\bar{m}}(\xi)L_{\bar{n}}(\eta) \\ &\psi^u_{pq}(\xi,\eta) = \psi^v_{pq}(\xi,\eta) = (\beta_1^2-\xi^2)^2 L_p(\xi)L_q(\eta) \\ &g_{mn}(\xi,\eta) = \frac{\mathrm{d}X^w_m(-\beta_1)}{\mathrm{d}\xi}Y^w_n(\eta)\frac{\beta_1-\xi}{2\beta_1} + \frac{\mathrm{d}X^w_m(\beta_1)}{\mathrm{d}\xi}Y^w_n(\eta)\frac{\xi+\beta_1}{2\beta_1} \\ &h_{mn}(\xi,\eta) = X^w_m(-\beta_1)\frac{\mathrm{d}Y^w_n(\eta)}{\mathrm{d}\eta}\frac{\beta_1-\xi}{2\beta_1} + X^w_m(\beta_1)\frac{\mathrm{d}Y^w_n(\eta)}{\mathrm{d}\eta}\frac{\xi+\beta_1}{2\beta_1} \end{aligned} \tag{22}$$

where $\beta_1 = c/a$. c is the length of through-the-width delamination, as shown in Fig. 2(a). Both global and local shape functions of the VAT plate with an embedded rectangular delamination are given by

$$\begin{aligned} &X^w_m(\xi)Y^w_n(\eta) = (1-\xi^2)(1-\eta^2)L_m(\xi)L_n(\eta) \\ &\psi^w_{\bar{m}\bar{n}}(\xi,\eta) = (\beta_1^2-\xi^2)^2(\beta_2^2-\eta^2)^2 L_{\bar{m}}(\xi)L_{\bar{n}}(\eta) \\ &\psi^u_{pq}(\xi,\eta) = \psi^v_{pq}(\xi,\eta) = (\beta_1^2-\xi^2)^2(\beta_2^2-\eta^2)^2 L_p(\xi)L_q(\eta) \\ &g_{mn}(\xi,\eta) = \frac{\mathrm{d}X^w_m(-\beta_1)}{\mathrm{d}\xi}Y^w_n(\eta)\frac{\beta_1-\xi}{2\beta_1} + \frac{\mathrm{d}X^w_m(\beta_1)}{\mathrm{d}\xi}Y^w_n(\eta)\frac{\xi+\beta_1}{2\beta_1} \\ &h_{mn}(\xi,\eta) = X^w_m(\xi)\frac{\mathrm{d}Y^w_n(-\beta_2)}{\mathrm{d}\eta}\frac{\beta_2-\eta}{2\beta_2} + X^w_m(\xi)\frac{\mathrm{d}Y^w_n(\beta_2)}{\mathrm{d}\eta}\frac{\eta+\beta_2}{2\beta_2} \end{aligned} \tag{23}$$

where $\beta_2 = c/b$. Note that, both length and width of embedded delamination are c, as shown in

Fig. 2(b).

According to Hamilton's principle,

$$\int_{t_1}^{t_2}\left(\delta T-\delta U+\delta V\right)\mathrm{d}t=0 \tag{24}$$

and substituting Eqs. (18)-(20) into Eq. (24), the equation of motion of VAT composite plates with a single delamination under periodically varying uniform axial compression is then solved by a Rayleigh-Ritz procedure and expressed in the following matrix form,

$$\mathbf{M}\ddot{\mathbf{q}}+\mathbf{K}\mathbf{q}-\left(\alpha_{\mathrm{S}}u_{\mathrm{cr}}+\alpha_{\mathrm{D}}u_{\mathrm{cr}}\cos(\Omega t)\right)\mathbf{G}\mathbf{q}=\mathbf{0} \tag{25}$$

where $\mathbf{q}$ is the time-dependent vector, that is,

$$\mathbf{q}=\{\mathbf{U}_{\mathbf{pq}}^{\mathbf{1}}\quad\mathbf{V}_{\mathbf{pq}}^{\mathbf{1}}\quad\mathbf{U}_{\mathbf{pq}}^{\mathbf{2}}\quad\mathbf{V}_{\mathbf{pq}}^{\mathbf{2}}\quad\mathbf{W}_{\mathbf{mn}}^{\mathbf{0}}\quad\mathbf{W}_{\bar{\mathbf{m}}\bar{\mathbf{n}}}^{\mathbf{1}}\quad\mathbf{W}_{\bar{\mathbf{m}}\bar{\mathbf{n}}}^{\mathbf{2}}\}^{\mathbf{T}}$$

$\mathbf{M}$, $\mathbf{K}$ and $\mathbf{G}$ are the mass, elastic stiffness and geometric stiffness matrices of the delaminated VAT composite plate, respectively, and expressed as

$$\mathbf{M}=\begin{bmatrix}\mathbf{0}&\mathbf{0}&\mathbf{0}&\mathbf{0}&\mathbf{0}&\mathbf{0}&\mathbf{0}\\\mathbf{0}&\mathbf{0}&\mathbf{0}&\mathbf{0}&\mathbf{0}&\mathbf{0}&\mathbf{0}\\\mathbf{0}&\mathbf{0}&\mathbf{0}&\mathbf{0}&\mathbf{0}&\mathbf{0}&\mathbf{0}\\\mathbf{0}&\mathbf{0}&\mathbf{0}&\mathbf{0}&\mathbf{0}&\mathbf{0}&\mathbf{0}\\\mathbf{0}&\mathbf{0}&\mathbf{0}&\mathbf{0}&\mathbf{M}_{\mathbf{W_0W_0}}&\mathbf{0}&\mathbf{0}\\\mathbf{0}&\mathbf{0}&\mathbf{0}&\mathbf{0}&\mathbf{0}&\mathbf{M}_{\mathbf{W_1W_1}}&\mathbf{0}\\\mathbf{0}&\mathbf{0}&\mathbf{0}&\mathbf{0}&\mathbf{0}&\mathbf{0}&\mathbf{M}_{\mathbf{W_2W_2}}\end{bmatrix},\quad \mathbf{G}=\begin{bmatrix}\mathbf{0}&\mathbf{0}&\mathbf{0}&\mathbf{0}&\mathbf{0}&\mathbf{0}&\mathbf{0}\\\mathbf{0}&\mathbf{0}&\mathbf{0}&\mathbf{0}&\mathbf{0}&\mathbf{0}&\mathbf{0}\\\mathbf{0}&\mathbf{0}&\mathbf{0}&\mathbf{0}&\mathbf{0}&\mathbf{0}&\mathbf{0}\\\mathbf{0}&\mathbf{0}&\mathbf{0}&\mathbf{0}&\mathbf{0}&\mathbf{0}&\mathbf{0}\\\mathbf{0}&\mathbf{0}&\mathbf{0}&\mathbf{0}&\mathbf{L}_{\mathbf{W_0W_0}}&\mathbf{L}_{\mathbf{W_0W_1}}&\mathbf{L}_{\mathbf{W_0W_2}}\\\mathbf{0}&\mathbf{0}&\mathbf{0}&\mathbf{0}&\mathbf{L}_{\mathbf{W_1W_0}}&\mathbf{L}_{\mathbf{W_1W_1}}&\mathbf{0}\\\mathbf{0}&\mathbf{0}&\mathbf{0}&\mathbf{0}&\mathbf{L}_{\mathbf{W_2W_0}}&\mathbf{0}&\mathbf{L}_{\mathbf{W_2W_2}}\end{bmatrix}$$

$$\mathbf{K}=\begin{bmatrix}\mathbf{K}_{\mathbf{U_1U_1}}&\mathbf{K}_{\mathbf{U_1V_1}}&\mathbf{0}&\mathbf{0}&\mathbf{K}_{\mathbf{U_1W_0}}&\mathbf{0}&\mathbf{0}\\\mathbf{K}_{\mathbf{V_1U_1}}&\mathbf{K}_{\mathbf{V_1V_1}}&\mathbf{0}&\mathbf{0}&\mathbf{K}_{\mathbf{V_1W_0}}&\mathbf{0}&\mathbf{0}\\\mathbf{0}&\mathbf{0}&\mathbf{K}_{\mathbf{U_2U_2}}&\mathbf{K}_{\mathbf{U_2V_2}}&\mathbf{K}_{\mathbf{U_2W_0}}&\mathbf{0}&\mathbf{0}\\\mathbf{0}&\mathbf{0}&\mathbf{K}_{\mathbf{V_2U_2}}&\mathbf{K}_{\mathbf{V_2V_2}}&\mathbf{K}_{\mathbf{V_2W_0}}&\mathbf{0}&\mathbf{0}\\\mathbf{K}_{\mathbf{W_0U_1}}&\mathbf{K}_{\mathbf{W_0V_1}}&\mathbf{K}_{\mathbf{W_0U_2}}&\mathbf{K}_{\mathbf{W_0V_2}}&\mathbf{K}_{\mathbf{W_0W_0}}&\mathbf{K}_{\mathbf{W_0W_1}}&\mathbf{K}_{\mathbf{W_0W_2}}\\\mathbf{0}&\mathbf{0}&\mathbf{0}&\mathbf{0}&\mathbf{K}_{\mathbf{W_1W_0}}&\mathbf{K}_{\mathbf{W_1W_1}}&\mathbf{0}\\\mathbf{0}&\mathbf{0}&\mathbf{0}&\mathbf{0}&\mathbf{K}_{\mathbf{W_2W_0}}&\mathbf{0}&\mathbf{K}_{\mathbf{W_2W_2}}\end{bmatrix}$$

The terms associated with the vector $\{\mathbf{U}_{\mathbf{pq}}^{\mathbf{1}}\quad\mathbf{V}_{\mathbf{pq}}^{\mathbf{1}}\quad\mathbf{U}_{\mathbf{pq}}^{\mathbf{2}}\quad\mathbf{V}_{\mathbf{pq}}^{\mathbf{2}}\}^{\mathbf{T}}$ in the elastic stiffness matrix are derived from the second part on the right hand side of Eq. (18). It is found that the vector $\{\mathbf{U}_{\mathbf{pq}}^{\mathbf{1}}\quad\mathbf{V}_{\mathbf{pq}}^{\mathbf{1}}\quad\mathbf{U}_{\mathbf{pq}}^{\mathbf{2}}\quad\mathbf{V}_{\mathbf{pq}}^{\mathbf{2}}\}^{\mathbf{T}}$ can be linearly represented by the vector $\left\{\mathbf{W}_{\mathbf{mn}}^{\mathbf{0}}\right\}^{\mathbf{T}}$. By means of matrix manipulation, Eq. (25) can be reduced to

$$\tilde{\mathbf{M}}\ddot{\Theta}+\tilde{\mathbf{K}}\Theta-\left(\alpha_{\mathrm{S}}u_{\mathrm{cr}}+\alpha_{\mathrm{D}}u_{\mathrm{cr}}\cos(\Omega t)\right)\tilde{\mathbf{G}}\Theta=\mathbf{0} \tag{26}$$

where Θ is the time-dependent vector, that is, $\Theta=\{\mathbf{W}_{\mathbf{mn}}^{\mathbf{0}}\quad\mathbf{W}_{\bar{\mathbf{m}}\bar{\mathbf{n}}}^{\mathbf{1}}\quad\mathbf{W}_{\bar{\mathbf{m}}\bar{\mathbf{n}}}^{\mathbf{2}}\}^{\mathbf{T}}$. Additionally, the modified stiffness matrices $\tilde{\mathbf{M}}$, $\tilde{\mathbf{K}}$ and $\tilde{\mathbf{G}}$ are expressed as

$$\tilde{\mathbf{M}}=\begin{bmatrix}\mathbf{M}_{\mathbf{W_0W_0}}&\mathbf{0}&\mathbf{0}\\\mathbf{0}&\mathbf{M}_{\mathbf{W_1W_1}}&\mathbf{0}\\\mathbf{0}&\mathbf{0}&\mathbf{M}_{\mathbf{W_2W_2}}\end{bmatrix},\quad \tilde{\mathbf{G}}=\begin{bmatrix}\mathbf{G}_{\mathbf{W_0W_0}}&\mathbf{G}_{\mathbf{W_0W_1}}&\mathbf{G}_{\mathbf{W_0W_2}}\\\mathbf{G}_{\mathbf{W_1W_0}}&\mathbf{G}_{\mathbf{W_1W_1}}&\mathbf{0}\\\mathbf{G}_{\mathbf{W_2W_0}}&\mathbf{0}&\mathbf{G}_{\mathbf{W_2W_2}}\end{bmatrix}$$

$$\tilde{\mathbf{K}}=\begin{bmatrix} \mathbf{K}_{W_0W_0}-\hat{\mathbf{K}}_{W_0W_0} & \mathbf{K}_{W_0W_1} & \mathbf{K}_{W_0W_2} \\ \mathbf{K}_{W_1W_0} & \mathbf{K}_{W_1W_1} & \mathbf{0} \\ \mathbf{K}_{W_2W_0} & \mathbf{0} & \mathbf{K}_{W_2W_2} \end{bmatrix}$$

$$\hat{\mathbf{K}}_{W_0W_0}=\begin{bmatrix} \mathbf{K}_{W_0U_1} & \mathbf{K}_{W_0V_1} & \mathbf{K}_{W_0U_2} & \mathbf{K}_{W_0V_2} \end{bmatrix}\begin{bmatrix} \mathbf{K}_{U_1U_1} & \mathbf{K}_{U_1V_1} & \mathbf{0} & \mathbf{0} \\ \mathbf{K}_{V_1U_1} & \mathbf{K}_{V_1V_1} & \mathbf{0} & \mathbf{0} \\ \mathbf{0} & \mathbf{0} & \mathbf{K}_{U_2U_2} & \mathbf{K}_{U_2V_2} \\ \mathbf{0} & \mathbf{0} & \mathbf{K}_{V_2U_2} & \mathbf{K}_{V_2V_2} \end{bmatrix}^{-1}\begin{bmatrix} \mathbf{K}_{U_1W_0} \\ \mathbf{K}_{V_1W_0} \\ \mathbf{K}_{U_2W_0} \\ \mathbf{K}_{V_2W_0} \end{bmatrix}$$

Note, the additional stiffness matrix $\hat{\mathbf{K}}_{W_0W_0}$ is critically important to accurately predict the buckling, vibration and dynamic instability response of delaminated VAT composite plates. Eq. (26) represents a system of differential equations with periodic coefficients of the Mathieu type, describing nonlinear instability behavior of the delaminated VAT composite plate. If harmonic and mass terms are neglected, Eq. (26) is then reduced to an eigenvalue equation governing the buckling problem, expressed as

$$(\tilde{\mathbf{K}}+\lambda\tilde{\mathbf{G}})\Theta=\mathbf{0} \tag{27}$$

where λ is the eigenvalue. The lowest eigenvalue λ_{cr} represents the critical buckling end-shortening value, that is, $\lambda_{cr}=u_{cr}$. Critical buckling loads of delaminated VAT composite plates are then evaluated by the following relation [1, 2, 4],

$$N_x^{cr}=\frac{\lambda_{cr}}{b}\int_{-b/2}^{b/2}\bar{N}_{xx}(y)\mathrm{d}y \quad \text{at} \quad x=\pm a/2 \tag{28}$$

If neglecting the third term on the left hand of Eq. (26), natural frequencies of delaminated VAT composite plates are obtained as

$$\tilde{\mathbf{M}}\ddot{\Theta}+\tilde{\mathbf{K}}\Theta=\mathbf{0} \tag{29}$$

In view of Eq. (29), both upper and lower delaminated portions deform freely without touching each other, and thus have independent transverse deformations. As such, the model described above is referred to as '*free model*'. However, the vibrational mode shape obtained using the free model may be physically inadmissible for an off-midplane delamination [20, 24, 44]. To address this problem, Mujumdar and Suryanarayan [20] proposed that both upper and lower delaminated portions are constrained to have identical transverse displacements. This model is called '*constrained model*' in contrast to the '*free model*'. In practice, however, delamination may breathe (open and close) during the period of the motion [22]. As illustrated in Fig. 4, the delamination opens when the delaminated beam vibrates upward, whereas the delamination remains closed when the delaminated beam vibrates downward. In the former case, the free model appears to the delaminated beam, as shown in Fig. 4 (a), while the latter case corresponds to the constrained one, as shown in Fig. 4 (c). Nevertheless, the above free and constrained models provide the lower and upper bounds of vibrational frequency for delaminated composite plates, respectively [23, 24]. To determine the upper bound of vibrational frequency for delaminated VAT composite plates, vibration analysis is therefore performed on the constrained model by

introducing an additional constraint condition, that is, $w^{(1)}=w^{(2)}$.

If only the harmonic term is neglected, Eq. (26) is then reduced to

$$\tilde{\mathbf{M}}\ddot{\Theta}+(\tilde{\mathbf{K}}-\alpha_S u_{cr}\tilde{\mathbf{G}})\Theta=\mathbf{0} \tag{30}$$

Solving Eq. (30), natural frequencies of delaminated VAT composite plates under the action of the static compressive loading are obtained.

This paper is mainly focused on the determination of instability boundaries for the principle dynamic instability region (DIR), which is of practical importance. To obtain points on the boundaries of the principle DIR, the solutions with period $2T$ ($T=2\pi/\omega$) of Eq. (26) can be written in the Fourier series [10]:

$$\Theta=\sum_{k=1,3,5}^{\infty}\left(\mathbf{a}_k\sin(k\Omega t/2)+\mathbf{b}_k\cos(k\Omega t/2)\right) \tag{31}$$

where $\mathbf{a}_k$ and $\mathbf{b}_k$ are the time-independent vectors and are infinite in number. Substituting Eq. (31) into Eq. (26) leads to infinite determinants [10]. However, approximate solutions can be obtained by truncating the Fourier series in Eq. (31), and a first order approximation is sufficient to accurately predict the upper and lower instability boundaries bounding the principle DIR [13, 14, 16-18]. Accordingly, in this work, the solution of Eq. (26) is approximated by

$$\Theta=\mathbf{a}_1\sin(\Omega t/2)+\mathbf{b}_1\cos(\Omega t/2) \tag{32}$$

By substituting the one-term series solutions into the Mathieu equation (26), the following simplified eigenvalue problems can be obtained and expressed as

$$[\tilde{\mathbf{K}}-(\alpha_S+0.5\alpha_D)u_{cr}\tilde{\mathbf{G}}]\{\mathbf{a}_1\}-0.25\Omega^2\tilde{\mathbf{M}}\{\mathbf{a}_1\}=0 \tag{33a}$$

$$[\tilde{\mathbf{K}}-(\alpha_S-0.5\alpha_D)u_{cr}\tilde{\mathbf{G}}]\{\mathbf{b}_1\}-0.25\Omega^2\tilde{\mathbf{M}}\{\mathbf{b}_1\}=0 \tag{33b}$$

Eqs. (33a) and (33b) determine the upper and lower instability boundaries of the principle DIR, respectively.

5 Results and discussions

In this section, numerical validation of VAT composite plates with a single delamination is performed by solving the buckling and vibration eigenvalue problems. Subsequently, results from dynamic instability analysis of delaminated VAT composite plates are presented in details. To verify the accuracy of the proposed analytical model, the behavior of VAT composite plates with a single delamination was simulated using commercial FEM software (Abaqus). A subroutine was developed to generate composite elements with independent fibre orientations. The SC8R shell element was chosen for the prebuckling, buckling and vibration analysis of delaminated VAT composite plates. To achieve the required accuracy, very fine meshes (60×60×16) were selected. In the delamination modelling, two sets of collocated shells, each of which represents an intact sublaminate, were incorporated into the FE model. The nodal displacements of two adjacent surfaces of the two sublaminates over the undelaminated region were tied using the multi-point constraints (MPCs). To facilitate the comparison of the numerical results, the following three

notations are defined: Normalized Delamination Position (NDP=h_1/h); Normalized Delamination Length (NDL=c/a) and Normalized Delamination Area (NDA=c^2/ab).

5.1 Model validation

Buckling analysis is first performed on a simply supported beam-plate with a through-the-width delamination, which was initially studied by Simitses et al. [41]. As shown in Table 1, the critical buckling loads predicted using the present Rayleigh-Ritz model for this delaminated beam-plate correlated with the results given by Simitses et al. [41] and FEM.

Subsequently, vibration analysis using the present Rayleigh-Ritz model is verified on a clamped beam-plate problem with a through-the-width delamination, which was studied by Wang et al. [19]. In this study, only *free model* is considered. The non-dimensional natural frequencies of delaminated beam-plates are compared with the results given by Wang et al. [19], Lee [22] and FEM. Excellent agreement between these predicted results has arrived, as shown in Table 2.

A further verification of vibration analysis is performed on a T300/934 graphite/epoxy cantilever beam-plate with a $[0/90]_{2s}$ stacking sequence, which was also studied in Shen et al.'s work [21]. The length and width of the cantilever beam-plate are a=127mm and b=12.7mm, respectively. The lamina properties are E_{11}=134.5GPa, E_{22}=10.3GPa, G_{12}=5.0GPa, v_{12}=0.33 and ρ=1480Kg/m^3 with ply thickness that is 0.127mm. Note, the bending-extension coupling within each delaminated portion is taken into account using the method of reduced bending stiffness (RBS) [36]. Four different positions for the delamination (as also denoted by interface 1, 2, 3 and 4 in [21]) with NDP=0.5, 0.375, 0.25 and 0.125 are considered, respectively. Five different sizes (length) for the delamination with NDL= 0.0 (intact), 0.2, 0.4, 0.6 and 0.8 are chosen to study, respectively. Herein, *both free and constrained models* are applied to predict the natural frequencies of delaminated beam-plates. Tables 3-6 list the fundamental frequencies of cantilever beam-plates with delamination for different NDP/NDL combinations. The results obtained using present method are compared with those given by Shen and Grady [21], Luo and Hanagud [23], Shu and Della [24, 44], and the FEM simulation, as shown in Tables 3-6. From Tables 3-5, it is clearly seen that the fundamental frequencies predicted by the present *free and constrained models* are in good agreement with experimental results [21], analytical results [23, 24, 44] and FEM results. However, it was also observed from Table 6 that there is a big discrepancy between the experimental results [21] and other results for the case that NDP=0.125. This is an experimental error, which is indicated by Luo and Hanagud [23].

In the *free model*, no delamination opening within the delamination region was found when the delamination interface is closed to the mid-plane (NDP=0.5 and NDP=0.375). Under such circumstance, the free and constrained models are essentially the same and thus give identical results of fundamental frequencies, as shown in Tables 3 and 4. However, when the delamination layer is off the mid-plane (NDP=0.25 and NDP=0.125), the upper and lower delaminated portions in the *free model* were found to separate from each other. This opening mode becomes more apparent with the increasing of delamination length (NDL value). The vibrational mode shapes

along the x-axis (y=0.0) for the cases with an off mid-plane delamination (NDP=0.125) with four different delamination sizes (NDL=0.2, 0.4, 0.6 and 0.8) are obtained using the present free model, and plotted in Fig. 5. It is clearly seen that there is a transition from closed to open in the vibrational mode shape with the increasing NDL value. Luo and Hanagud arrived at the similar conclusion in [23]. Therefore, the *free model* and the *constrained model* will lead to different results in the vibration analysis of delaminated beam-plates when the delamination interface is off the mid-plane. Such difference will be enlarged with the increasing of delamination size (NDL value).

In the present work, for VAT configurations, up to 6^{th} order Legendre polynomials in the expression of Eqs. (14) and (16) were taken to determine the non-uniform in-plane stress distribution, accurately. Besides, it was found that 7^{th} order Legendre polynomials for both global and local displacement shape functions in the expression of Eq. (22) are needed to obtain the convergent results for the buckling, free vibration and dynamic instability analysis.

5.2 Buckling and vibration response of delaminated VAT plates

The buckling and vibration response of VAT composite plates with an embedded rectangular delamination is studied in this section. The length and width of VAT laminates are both a=b=814mm. The material properties of lamina are E_{11}=181GPa, E_{22}=10.3GPa, G_{12}=7.17GPa, v_{12}=0.28 and ρ=1540Kg/m^3 and the thickness of each ply equals to 0.127mm. The laminate layup of VAT composite plates is chosen to be $[\pm\langle 0,30\rangle]_{4s}$ and the boundary conditions are simply supported at all four edges. In the buckling analysis, the delaminated VAT plate is loaded by a uniform displacement compression with transverse edges free to deform.

The bucking coefficient of the delaminated VAT composite plate is defined as [1, 2, 4]

$$K_{\mathrm{cr}} = \frac{N_x^{\mathrm{cr}} a^2}{E_{11} h^3} \tag{34}$$

In Fig. 6, the buckling coefficient of delaminated VAT plate that varies with respect to the delamination size (NDA) are plotted for two different delamination positions, that is, NDP=0.25 and NDP=0.5. As shown in Fig. 6, results predicted by the present analytical model show excellent agreement with FEM results. It is clearly seen that the buckling coefficient initially remains almost constant and then gradually decreases with the increase of delamination size (NDA). Further, it is observed that the reduction of buckling coefficient for the off mid-plane delamination case (NDP=0.25) is more pronounced than that of the mid-plane delamination (NDP=0.5). For the former case, the thinner and thicker delaminated portions were found to separate from each other when the delamination size (NDA) becomes large. Therefore, the delamination results in an opening mode shape, which significantly reduces the buckling coefficient. A detailed study on the buckling behavior of delaminated VAT composite plates had been presented in our previous works [43].

The natural frequency of the delaminated VAT composite plate is normalized and defined as [18,

28]

$$\tilde{\omega} = \frac{a^2}{h}\sqrt{\frac{\rho}{E_{22}}}\omega \tag{35}$$

Table 7 lists normalized natural frequencies obtained using *both the free and constrained models* for different NDP/NDA combinations. FEM results based on the *free model* are obtained and included for the purpose of comparison. As presented in Table 7, results given by the proposed *free model* and FE analysis are found to be in good agreement. From Table 7, it is clearly seen that for *both free and constrained models*, the normalized natural frequency $\tilde{\omega}$ initially remains unchanged, and subsequently decreases with the increase of delamination size (NDA). It is further observed that the normalized natural frequency $\tilde{\omega}$ obtained using the *constrained model* is reduced more severely for the midplane delamination case (NDP=0.5) than that of the off-midplane delamination (NDP=0.25). This is because that the delamination opening mode is not considered in the *constrained model* even for an off-midplane delamination (NDP=0.25). In this case, the loss of bending stiffness within the delamination region is the only reason for the decrease of natural frequency. The closer to the midplane, the delamination interface results in more loss of bending stiffness. However, the reduction of natural frequency predicted by the *free model* is more prominent for the off-midplane delamination case (NDP=0.25) than that of the midplane delamination (NDP=0.5). In this case, natural frequencies obtained for NDP = 0.25 may be further reduced by the occurrence of opening mode shape when the delamination size (NDA) becomes relatively large.

Fig. 7 compares vibrational mode shapes of the delaminated VAT laminate $[\pm\langle 0,30\rangle]_{4s}$ for different NDP/NDA combinations predicted by the analytical method and FEM (based on the *free model*). Two different delamination positions (NDP=0.25 and 0.5) and four different delamination sizes (NDA=0.0, 0.25, 0.49 and 0.81) are considered herein. As shown in Fig. 7, vibrational mode shapes obtained using the present *free model* match very well with FE results. For the case of midplane delamination (NDP=0.5), both delaminated portions deform by the same amount and there is no delamination opening observed during the period of the motion. For this case (midplane delamination), *the free and constrained models* are essentially the same and thus natural frequencies obtained using these two models are identical, as illustrated in Table 7. However, for the case of an off-midplane delamination (NDP=0.25), the upper and lower delaminated portions separate from each other (delamination opening occurs) when the delamination size is gradually increased. Note, there remains a risk that the vibrational mode shapes predicted by the *free model* for the off mid-plane delamination case are physically inadmissible. In this case, the bending stiffness of the thinner delaminated portion is much smaller than that of the thicker portion. Therefore, the amplitude of the vibration in the thinner delaminated portion is much larger than that of the thicker one. As a result, natural frequencies predicted by the present *free model* are significantly affected by the occurrence of delamination opening, especially for a large delamination size (NDA), as illustrated in Table 7.

Subsequently, the influence of static in-plane compressive load on the natural frequencies of delaminated VAT composite plates is studied. Only the mid-plane delamination (NDP=0.5) is considered in this study. The delaminated VAT composite plate is loaded by uniform axial compression with the static load parameter α_S ranging from 0.0 to 1.0. Note, α_S=0.0 denotes the state of free vibration for delaminated VAT composite plates; α_S=1.0 indicates that the delaminated VAT composite plates have already buckled. The variation of normalized natural frequency $\tilde{\omega}$ with respect to the static in-plane compressive load $\alpha_S K_{cr}$ for four different delamination sizes (NDA=0.0, 0.25, 0.49 and 0.81) are plotted in Fig. 8, and validated with FEM results. It is observed that the natural frequency $\tilde{\omega}$ decreases with increasing the static in-plane compressive load $\alpha_S K_{cr}$.

5.3 Dynamic instability response of delaminated VAT plates

This section presents the dynamic instability analysis of delaminated VAT composite plates under periodically varying uniform axial compression. The delaminated VAT plates are simply supported at all four edges. Since only an embedded rectangular midplane delamination is considered, both the opening problem and contact problem [37, 40] are not taken into account in the dynamic instability analysis. The influence of delamination size, static load parameter and varying fibre orientation angle on the dynamic instability response of delaminated VAT composite plates will be studied in details.

5.3.1 Effect of delamination size

This section studies the effect of delamination size on the dynamic instability response of delaminated VAT composite plates. The VAT laminate plates $[\pm\langle 0,30\rangle]_{4s}$ with four different delamination sizes (NDA=0.0, 0.25, 0.49 and 0.81) are examined in the analysis. The static load parameter α_S is set to be 0.0, while the dynamic load parameter α_D increases from 0.0 to 1.0. The boundary resonance frequencies are normalized using Eq. (35), in which the natural frequency ω is replaced by the excitation frequency Ω.

The upper and lower boundary resonance frequencies ($\tilde{\Omega}$) of VAT composite plates with different delamination sizes (NDA) are obtained and plotted in Fig. 9 (a), with respect to the dynamic in-plane compressive load ($\alpha_D K_{cr}$). Note, the value of $\alpha_D K_{cr}$ equals to the critical buckling coefficient at α_D=1.0, beyond which the delaminated VAT composite plates are completely unstable. The principal DIR of each delaminated VAT composite plate shown in Fig. 9 (a) starts at a tip point where the parametric resonance frequency is twice its fundamental natural frequency. From Fig. 9 (a), it is observed that the increase of delamination size (NDA) leads to: (1) early onset of instability and wider DIR; (2) the principal DIR is shifted towards lower parametric resonance frequencies; (3) the curves bounding the principle DIR are reduced to a smaller range of the dynamic in-plane compressive load ($\alpha_D K_{cr}$). This is mainly attributed to the reduction of natural frequency and critical buckling load induced by the occurrence of delamination. These numerical results indicate that the delaminated VAT composite plate becomes much more dynamic

unstable when the delamination size is increased.

The dynamic instability of a composite laminate is closely related to its fundamental natural frequency and critical buckling load [16]. Thus, a dynamic instability index (DII) is defined to characterize the dynamic instability performance of delaminated VAT composite plates and represented as [16, 18]

$$\mathrm{DII} = \frac{\mathrm{DIO}}{\omega K_{\mathrm{cr}}} \tag{36}$$

where DIO, known as the dynamic instability opening, is the distance between the two boundaries of the DIR. It represents the range of the parametric resonance frequency at a specific dynamic load parameter α_D [12, 16]. A larger value of DII indicates that the plate is more dynamically unstable. The DII value of the delaminated VAT plate $[\pm\langle 0,30\rangle]_{4s}$ at α_D=0.4 that varies with respect to the delamination size (NDA) is plotted in Fig. 9 (b). As shown in Fig. 9 (b), with the increase in delamination size (NDA), the DII value dramatically increases, and thus the delaminated VAT plate becomes more dynamically unstable. The primary reason is attributed to the reduction in natural frequency and critical buckling load and the increase of DIO value for an increasing delamination size.

5.3.2 Effect of static load parameter

The influence of the static in-plane compressive load on the dynamic instability response of delaminated VAT composite plates is studied in this section. The static load parameter α_S increases from 0.0 to 0.6 with a step of 0.2, while the dynamic load parameter α_D varies from 0.0 to 1.0. The boundary resonance frequencies of the delaminated VAT plate $[\pm\langle 0,30\rangle]_{4s}$ with a large delamination size (NDA=0.49) under four different static load parameters (α_S=0.0, 0.2, 0.4 and 0.6) are obtained and plotted in Fig. 10 (a). As shown in Fig. 10 (a), the principal DIR of the delaminated VAT plate $[\pm\langle 0,30\rangle]_{4s}$ becomes wider and shifted to lower frequency when the static load parameter α_S is increased. For the case of α_S=0.6, the lower resonance frequency boundary terminates at $\alpha_D K_{cr}$=0.89, beyond which the delaminated VAT composite plate becomes completely unstable. This implies that the presence of the static in-plane compressive load further leads to significant dynamic instability of the delaminated VAT plate.

The variation of the DII value evaluated at α_D=0.3 with respect to the static load parameter α_S is plotted in Fig. 10 (b). It is found that the DII value is dramatically increased with increasing the static load parameter α_S. It thus indicates that a higher static compressive load leads to a larger instability of delaminated VAT plates.

5.3.3 Effect of varying fibre orientation angles

Dynamic instability analysis is then performed on the delaminated VAT layups $[90\pm\langle T_0,T_1\rangle]_{4s}$ with linear variation of fibre angles. Firstly, the influence of fibre orientation angles on the principal dynamic instability region (DIR) of delaminated VAT plates $[90\pm\langle 0,T_1\rangle]_{4s}$ is studied in details. Herein, T_1 increases from 0° to 80° with an incremental step of 20°. The static load

parameter α_S is set to be 0.0, while the dynamic load parameter α_D increases from 0.0 to 1.0.

The DIRs of the delaminated VAT plates $[90\pm\langle 0,T_1\rangle]_{4s}$ for four different delamination sizes (NDA=0.0, 0.25, 0.49 and 0.81) are evaluated and plotted in Fig. 11. It is clearly seen that for these VAT layups, the increase of delamination size (NDA value) leads to an early onset of dynamic instability. This is due to the reduction of natural frequency of VAT plates induced by the occurrence of delamination. However, the instability onset of VAT laminates starts at a higher resonance frequency than that of straight-fiber laminates even if there exists a delamination. For instance, when NDA=0.49, the VAT layup $[90\pm\langle 0,60\rangle]_{4s}$ shows an improvement of 25.7% over the straight-fibre layup $[90\pm\langle 0,0\rangle]_{4s}$. With an increase of NDA value, the principle DIR of each layup tends to be wider and shifted towards lower parametric resonance frequencies, and the two curves bounding the principle DIR extend to a smaller range of the dynamic in-plane compressive load ($\alpha_D K_{cr}$). It implies that VAT composite plates become more dynamically unstable when the delamination size is increased. At different NDA values, the boundaries of the principle DIR for the VAT plate $[90\pm\langle 0,80\rangle]_{4s}$ have the largest extension in terms of the dynamic in-plane compressive load ($\alpha_D K_{cr}$), indicating that the VAT layup $[90\pm\langle 0,80\rangle]_{4s}$ achieves better dynamic stability performance than other layups. This also implies that the dynamic stability can be significantly improved through introducing the VAT concept. Load redistribution that is away from the center of the plate towards transverse boundary edges is the primary mechanism for this substantial improvement in critical buckling load, which therefore enables the VAT layup $[90\pm\langle 0,80\rangle]_{4s}$ to achieve better dynamic stability performance. This mechanism remains in effect even if there exists a delamination.

The DII values of the delaminated VAT plates $[90\pm\langle T_0,T_1\rangle]_{4s}$ are then predicted by the proposed method. In this case, both T_0 and T_1 increase from 0° to 90° with an incremental step of 10°. The static load parameter α_S and dynamic load parameter α_D are set to be 0.0 and 0.3, respectively. For comparison purposes, the DII and prebuckling stiffness E_{vat} of delaminated VAT plates are normalized with respect to those of an intact quasi-isotropic laminate, respectively. The prebuckling stiffness E_{vat} is defined as [1, 2, 4]

$$E_{vat} = \frac{a}{hb^2\Delta}\int_{-b/2}^{b/2} N_{xx}^{(0)}(a/2, y)\mathrm{d}y \tag{37}$$

And the evaluation of DII value of the intact quasi-isotropic laminate is based on an equivalent bending stiffness, given by [4, 7],

$$D_{iso} = \frac{E_{iso}}{12(1-\nu_{iso}^2)}, \nu_{iso} = \frac{U_4}{U_1}, E_{iso} = U_1(1-\nu_{iso}^2) \tag{38}$$

where ν_{iso} and E_{iso} are the equivalent Poisson's ratio and equivalent Young' modulus, respectively.

Fig. 12 shows the normalized DII value versus normalized prebuckling stiffness for all VAT configurations with four different delamination sizes (NDA), namely, 0.0, 0.25, 0.49 and 0.81. Each curve is generated by varying T_1 from 0° at the left-end to 90° at the right-end for a given value of T_0. As shown in Fig. 12, for all VAT configurations, the normalized DII value increases

with an increase of the delamination size (NDA). It thus indicates that the delaminated VAT plates become more dynamically unstable when the delamination size is increased. The reduction of natural frequency and critical buckling load of laminated plates and the increase of DIO value, induced by the occurrence of delamination, eventually lead to the increase of DII values. However, it was found that the VAT layup $[90\pm\langle 0,80\rangle]_{4s}$ gives the minimum DII value for all the delamination sizes. At each NDA value of 0.0, 0.25, 0.49 and 0.81, the minimum DII value of the VAT layup $[90\pm\langle 0,80\rangle]_{4s}$ shows an improvement of 44.4%, 46.3%, 50.7% and 49.4% over that given by the straight-fiber laminate $[\pm 45]_{4s}$, respectively. As explained previously, the benign non-uniform load redistribution given rise by the non-uniform extensional stiffness is the major reason for the VAT layup $[90\pm\langle 0,80\rangle]_{4s}$ to achieve the maximum critical buckling load and the minimum DII value. This also implies that the benign load redistribution induced by the variable stiffness properties is more critical to this substantial improvement in dynamic stability. In addition, as shown in Fig. 12, when the normalized prebuckling stiffness is between 0.4 and 1.6, the VAT layups offer additional freedom in stiffness tailoring to achieve improved dynamic stability performance for composite laminated plates, even the delamination occurs. These results clearly demonstrate the distinct superiority of applying variable stiffness properties to enhance the dynamic stability response of composite laminated plates with a single delamination.

6 Conclusions

In this study, an improved analytical model was developed to perform the dynamic instability analysis of VAT composite plates with a single delamination subjected to periodically varying in-plane compressive loading. The equations of motion associated with dynamic instability were derived using Hamilton's principle, and the dynamic instability regions were determined using Bolotin's approach. The Rayleigh-Ritz approach was adopted to solve the in-plane stress distribution and dynamic instability problems. Results of buckling loads and natural frequencies obtained by the proposed method well matched with previous published results and FEA results. The following conclusions were arrived from the analysis:

(1) Critical buckling loads decrease with the increase of delamination size. Such reduction is more pronounced for composite laminates with an off-midplane delamination;

(2) Natural frequencies also decrease with the increase of delamination size. Such reduction for composite laminates with a mid-plane delamination is more pronounced when the delamination problem is modelled by the constrained model. However, for laminates with an off-midplane delamination, such reduction is more pronounced when the free model is used;

(3) The increase of delamination size leads to an early onset of the dynamic instability. With the increasing of delamination size, the dynamic instability regions are shifted to lower parametric resonance frequencies and lessened to a smaller range with respect to in-plane compressive load;

(4) The dynamic instability of delaminated VAT plates is further reduced when a static in-plane compressive loading is applied;

(5) Substantial improvement of dynamic stability performance of delaminated VAT composite

plates is achieved when the majority of compressive load is redistributed to the supported edges;

(6) Compared to the straight-fibre laminates, the VAT laminates offer additional freedom in stiffness tailoring to achieve improved dynamic stability performance against the occurrence of delamination.

Acknowledgments

Zhangming Wu would like to acknowledge the financial support from China's 1000 young scholarship plan, and the Strathclyde Chancellor's Fellowship (University of Strathclyde, Scotland). This work was also partially supported by the National Natural Science Foundation of China (No. 11372225 and 11072177).

Reference

[1] Gürdal Z, Tatting BF, Wu CK. Variable stiffness composite panels: Effects of stiffness variation on the in-plane and buckling response. Composites Part A 2008; 39(5): 911-22.

[2] Raju G, Wu Z, Kim BC, Weaver PM. Prebuckling and buckling analysis of variable angle tow plates with general boundary conditions. Composite Structures 2012; 94(9): 2961-70.

[3] Setoodeh S, Abdalla MM, IJsselmuiden ST, Gürdal Z. Design of variable-stiffness composite panels for maximum buckling load. Composite Structures 2009; 87(1): 109-17.

[4] Wu Z, Weaver PM, Raju G, Kim BC. Buckling analysis and optimisation of variable angle tow composite plates. Thin-Walled Structures 2012; 60(10): 163-72.

[5] Zucco G, Groh RMJ, Madeo A, Weaver PM. Mixed shell element for static and buckling analysis of variable angle tow composite plates. Composite Structures 2016; 152: 324-38.

[6] Raju G, Wu ZM, Weaver PM. Buckling and postbuckling of variable angle tow composite plates under in-plane shear loading. International Journal of Solids and Structures 2015; 58: 270-87.

[7] Wu Z, Raju G, Weaver PM. Postbuckling analysis of variable angle tow composite plates. International Journal of Solids and Structures 2013; 50(10): 1770-80.

[8] Akhavan H, Ribeiro P. Natural modes of vibration of variable stiffness composite laminates with curvilinear fibers. Composite Structures 2011; 93(11): 3040-7.

[9] Henson MC, Wang BP. Vibration and buckling of quadrilateral variable stiffness laminated composite plates. In: 57th AIAA/ASCE/AHS/ASC Structures, Structural Dynamics, and Materials Conference; 2016. p. 1-18.

[10] Bolotin VV. The dynamic stability of elastic systems. San Francisco, CA: Holden-Day; 1964.

[11] Birman V. Dynamic stability of unsymmetrically laminated rectangular plates. Mechanics Research Communications 1985; 12(2): 81-6.

[12] Srinivasan RS, Chellapandi P. Dynamic stability of rectangular laminated composite plates. Computers Structures 1986; 24(2): 233-38.

[13] Moorthy J, Reddy JN. Parametric instability of laminated composite plates with transverse shear deformation. International Journal of Solids and Structures 1990; 26(7): 801-11.

[14] Chattopadhyay A, Radu AG. Dynamic instability of composite laminates using a higher order theory. Computers Structures 2000; 77(5): 453-60.

[15] Mond M, Cederbaum G. Dynamic instability of antisymmetric laminated plates. Journal of Sound and Vibration 1992; 154(2): 271-79.

[16] Wang S, Dawe DJ. Dynamic instability of composite laminated rectangular plates and prismatic plate structures. Computer Methods in Applied Mechanics and Engineering 2002; 191(17-18): 1791-826.

[17] Sahu SK, Datta PK. Dynamic instability of laminated composite rectangular plates subjected to non-uniform harmonic in-plane edge loading. Proceedings of the Institution of Mechanical Engineers Part G-Journal of Aerospace Engineering 2000; 214(5): 295-312.

[18] Samukham S, Raju G, Vyasarayani CP. Parametric instabilities of variable angle tow composite laminate under axial compression. Composite Structures 2017; 166: 229-38.

[19] Wang JTS, Liu YY, Gibby JA. Vibrations of split beams. Journal of Sound and Vibration 1982; 84(4): 491-502.

[20] Mujumdar PM, Suryanarayan S. Flexural vibrations of beams with delaminations. Journal of Sound and Vibration 1988; 125(3): 441-61.

[21] Shen MHH, Grady JE. Free vibrations of delaminated beams. AIAA Journal 1992; 30(5): 1361-70.

[22] Lee J. Free vibration analysis of delaminated composite beams. Computers Structures 2000; 74(2): 121-9.

[23] Luo H, Hanagud S. Dynamics of delaminated beams. International Journal of Solids and Structures 2000; 37(10): 1501-19.

[24] Shu D, Della CN. Vibrations of multiple delaminated beams. Composite Structures 2004; 64(3-4): 467-77.

[25] Alnefaie K. Finite element modeling of composite plates with internal delamination. Composite Structures 2009; 90(1): 21-7.

[26] Li D, Qing G. Free vibration analysis of composite laminates with delamination based on state space theory. Mechanics of Advanced Materials and Structures 2014; 21(5): 402-11.

[27] Liu Y, Shu D. Free vibration analysis of exponential functionally graded beams with a single delamination. Composites Part B-Engineering 2014; 59: 166-72.

[28] Mohanty J, Sahu SK, Parhi PK. Parametric instability of delaminated composite plates subjected to periodic in-plane loading. Journal of Vibration and Control 2015; 21(3): 419-34.

[29] Radu AG, Chattopadhyay A. Dynamic stability analysis of composite plates including delaminations using a higher order theory and transformation matrix approach. International Journal of Solids and Structures 2002; 39(7): 1949-65.

[30] Yang J, Fu Y. Analysis of dynamic stability for composite laminated cylindrical shells with delaminations. Composite Structures 2007; 78(3): 309-15.

[31] Park T, Lee SY. Parametric instability of delaminated composite spherical shells subjected to in-plane pulsating forces. Composite Structures 2009; 91(2): 196-204.

[32] Noh MH, Lee SY. Dynamic instability of delaminated composite skew plates subjected to combined static and dynamic loads based on HSDT. Composites Part B 2014; 58(58): 113-21.

[33] Fazilati J. Stability analysis of variable stiffness composite laminated platres with delamination using spline-FSM. Latin American Journal of Solids and Structures 2017; 14: 528-43.

[34] Gürdal Z, Olmedo R. In-plane response of laminates with spatially varying fiber orientations: Variable stiffness concept. AIAA Journal 1993; 31(4): 751-8.

[35] Reddy JN. Mechanics of laminated composite plates and shells theory and analysis. 2nd ed. New York: CRC press; 2004.

[36] Ashton JE. Approximate solutions for unsymmetrically laminated plates. Journal of Composite Materials 1969; 3(1): 189-91.

[37] Suemasu H, Kumagai T, Gozu K. Compressive behavior of multiply delaminated composite laminates part 1: Experiment and analytical development. AIAA Journal 1998; 36(7): 1279-85.

[38] Kardomateas GA, Schmueser DW. Buckling and postbuckling of delaminated composites under compressive loads including transverse shear effects. AIAA Journal 1988; 26(3): 337-43.

[39] Kharazi M, Ovesy HR, Mooneghi MA. Buckling analysis of delaminated composite plates using a novel layerwise theory. Thin-Walled Structures 2014; 74(1): 246-54.

[40] Shu D. Buckling of multiple delaminated beams. International Journal of Solids and Structures 1998; 35(13): 1451-65.

[41] Simitses GJ, Sallam S, Yin WL. Effect of delamination of axially loaded homogeneous laminated plates. AIAA Journal 1985; 23(9): 1437-44.

[42] Wu Z, Raju G, Weaver PM. Framework for the buckling optimization of variable angle tow composite plates. AIAA Journal 2015; 53(12): 3788-804.

[43] Chen X, Wu Z, Nie G, Weaver PM. Buckling analysis of variable angle tow composite plates with a through-the-width or an embedded rectangular delamination. International Journal of Solids and Structures 2017: Under Review.

[44] Della CN, Shu D. Vibration of delaminated composite laminates: A review. Applied Mechanics Reviews 2007; 60(1-6): 1-20.

Figure captions

Fig. 1 A delaminated VAT plate is divided into three portions by the delamination interface

Fig. 2 The in-plane boundary conditions of a VAT composite plate with a single delamination under periodically varying uniform axial compression: (a) VAT plate with a through-the-width delamination; (b) VAT plate with an embedded rectangular delamination

Fig. 3 Deformation process of delaminated portions along the delamination edge

Fig. 4 Two possible vibration mode shapes of a clamped beam-plate with an off-midplane delamination during the period of the motion

Fig. 5 Vibrational mode shapes of a cantilever beam-plate $[0/90]_{2s}$ obtained by the present free model while NDP=0.125 for different NDL values, that are 0.2, 0.4, 0.6 and 0.8.

Fig. 6 Buckling coefficient versus NDA value of the VAT composite plate $[\pm\langle 0,30\rangle]_{4s}$ with an embedded rectangular delamination with respect to two different delamination positions (NDP=0.5 and 0.25)

Fig. 7 Vibrational mode shapes of the VAT composite plate $[\pm\langle 0,30\rangle]_{4s}$ with an embedded rectangular delamination obtained using the free model for various NDP/NDA combinations

Fig. 8 Normalized natural frequency $\tilde{\omega}$ versus static in-plane compressive load $\alpha_S K_{cr}$ of the VAT composite plate $[\pm\langle 0,30\rangle]_{4s}$ with an embedded rectangular delamination obtained for four different NDA values, namely, 0.0, 0.25, 0.49 and 0.81

Fig. 9 Variation in dynamic instability with different NDA values for the VAT composite plate $[\pm\langle 0,30\rangle]_{4s}$ with an embedded rectangular delamination under periodically varying uniform axial compression. (a) Principle dynamic instability region (DIR) versus NDA value; (b) Dynamic instability index (DII) versus NDA value

Fig. 10 Variation in dynamic instability with the static load parameter for the VAT composite plate $[\pm\langle 0,30\rangle]_{4s}$ with an embedded rectangular delamination under periodically varying uniform axial compression. (a) Principle dynamic instability region (DIR) versus the static load parameter; (b) Dynamic instability index (DII) versus the static load parameter

Fig. 11 Principle dynamic instability regions of square simply supported VAT plates $[90\pm\langle 0,T1\rangle]4s$ with different fiber angles T_1 at four different NDA values, namely, 0.0, 0.25,0.49 and 0.81

Fig. 12 Normalized DII value versus normalized prebuckling stiffness of square simply supported VAT plates $[90\pm\langle T_0,T_1\rangle]_{4s}$ with different fiber angles T_0 and T_1 at four different NDA

values (0.0, 0.25,0.49 and 0.81).

Table

Table 1 Dimensionless critical buckling loads of a simply supported beam-plate with a through-the-width delamination for different NDP/NDL combinations

NDL	NDP=0.5			NDP=0.3		
	Present	Simitses [41]	FEM	Present	Simitses [41]	FEM
0.0	1.0000	1.0000	1.0000	1.0000	1.0000	1.0000
0.1	0.9999	0.9999	1.0000	0.9999	1.0000	0.9998
0.2	0.9997	0.9997	0.9997	0.9996	0.9997	0.9991
0.3	0.9979	0.9980	0.9981	0.9969	0.9971	0.9958
0.4	0.9912	0.9912	0.9909	0.9850	0.9827	0.9849
0.5	0.9726	0.9729	0.9728	0.9401	0.9402	0.9377
0.6	0.9345	0.9343	0.9345	0.8151	0.8149	0.8134
0.7	0.8706	0.8703	0.8705	0.6487	0.6484	0.6467
0.8	0.7870	0.7867	0.7867	0.5120	0.5118	0.5116
0.9	0.6970	0.6966	0.6965	0.4108	0.4106	0.4101

Table 2 The non-dimensional natural frequencies of a clamped beam-plate with a through-the-width delamination obtained using the proposed free model for different NDP/NDL combinations

NDL	NDP=0.5				NDP=0.25		
	Present	Wang [19]	Lee [22]	FEM	Present	Wang [19]	FEM
0.0	22.36	22.39	22.36	22.38	22.36	22.39	22.38
0.1	22.35	22.37	22.36	22.38	22.36	22.37	22.38
0.2	22.32	22.35	22.35	22.34	22.33	22.35	22.35
0.3	22.20	22.23	22.23	22.20	22.14	22.16	22.14
0.4	21.80	21.83	21.82	21.85	21.36	21.37	21.39
0.5	20.85	20.88	20.88	20.70	18.82	18.80	18.49
0.6	19.26	19.29	19.28	19.37	14.65	14.62	14.88
0.7	17.22	17.23	17.22	17.33	11.15	11.12	11.25
0.8	15.05	15.05	15.05	14.99	8.65	8.64	8.62
0.9	13.00	13.00	12.99	13.03	6.88	6.88	6.87

Table 3 Comparison of natural frequencies of a cantilever beam-plate $[0/90]_{2s}$ with a through-the-width delamination with NDP=0.5 (unit: Hz)

NDL	Present		Shen [21]	Luo [23]		Shu [24, 44]		FEM
	Free	Cons	Averaged test	Free	Cons	Free	Cons	Free
0.0	82.19	82.19	79.83	81.86	81.86	81.88	81.88	82.10
0.2	80.81	80.81	78.17	81.45	81.45	80.47	80.47	81.11
0.4	76.72	76.72	75.38	76.81	76.81	75.36	75.36	76.36
0.6	67.53	67.53	66.96	67.64	67.64	66.13	66.14	67.00
0.8	56.18	56.18	57.54	56.95	56.95	55.67	55.67	56.10

Table 4 Comparison of natural frequencies of a cantilever beam-plate $[0/90]_{2s}$ with a through-the-width delamination with NDP=0.375 (unit: Hz)

NDL	Present		Shen [21]	Luo [23]		Shu [24, 44]		FEM
	Free	Cons	Averaged test	Free	Cons	Free	Cons	Free
0.0	82.19	82.19	79.83	81.86	81.86	81.88	81.88	82.10
0.2	81.02	81.02	77.79	80.86	80.86	80.58	80.58	81.27
0.4	77.25	77.25	75.13	76.62	76.62	75.81	75.81	76.67
0.6	68.76	68.76	67.96	68.80	68.80	67.05	67.05	67.92
0.8	56.39	56.39	48.33	59.34	59.34	56.86	56.86	57.15

Table 5 Comparison of natural frequencies of a cantilever beam-plate $[0/90]_{2s}$ with a through-the-width delamination while NDP=0.25 (unit: Hz)

NDL	Present		Shen [21]	Luo [23]		Shu [24, 44]		FEM
	Free	Cons	Averaged test	Free	Cons	Free	Cons	Free
0.0	82.19	82.19	79.83	81.86	81.86	81.88	81.88	82.10
0.2	81.63	81.63	80.13	82.01	82.02	81.53	81.53	81.87
0.4	80.04	80.05	79.75	80.74	80.79	80.09	80.13	80.45
0.6	76.46	76.57	76.96	77.52	77.82	76.75	77.03	77.01
0.8	71.23	71.66	72.46	71.73	72.46	70.92	72.28	71.00

Table 6 Comparison of natural frequencies of a cantilever beam-plate $[0/90]_{2s}$ with a through-the-width delamination at NDP=0.125 (unit: Hz)

NDL	Present		Shen [21]	Luo [23]		Shu [24, 44]		FEM
	Free	Cons	Averaged test	Free	Cons	Free	Cons	Free
0.0	82.19	82.19	79.88	81.86	81.86	81.88	81.88	82.10
0.2	81.76	81.76	79.96	82.03	82.04	81.57	81.57	81.90
0.4	80.36	80.37	68.92	80.87	80.95	80.31	80.33	80.68
0.6	77.08	77.22	62.50	77.61	78.29	77.41	77.56	77.69
0.8	71.98	72.66	55.63	69.44	74.05	72.51	73.22	72.65

Table 7 The normalized natural frequencies of the VAT composite plate $[\pm\langle 0,30\rangle]_{4s}$ with an embedded rectangular delamination for different NDP/NDA combinations

NDA	NDP=0.5			NDP=0.25		
	R-R		FEM	R-R		FEM
	Free	Cons	Free	Free	Cons	Free
0.00	15.3593	15.3593	15.3214	15.3593	15.3593	15.3214
0.01	15.3593	15.3593	15.3214	15.3593	15.3593	15.3214
0.04	15.3580	15.3580	15.3190	15.3538	15.3611	15.3198
0.09	15.3470	15.3470	15.3063	15.3422	15.3468	15.2944
0.16	15.3039	15.3039	15.2635	15.2755	15.3346	15.2287
0.25	15.1588	15.1588	15.0639	15.0207	15.2704	14.8952
0.36	14.8039	14.8039	14.7510	14.2168	15.1107	14.1973
0.49	14.1289	14.1289	14.0745	12.3392	14.7893	12.3396
0.64	13.1253	13.1253	13.0772	9.9959	14.2555	9.9956
0.81	11.9068	11.9068	11.8770	8.0156	13.5065	7.9930

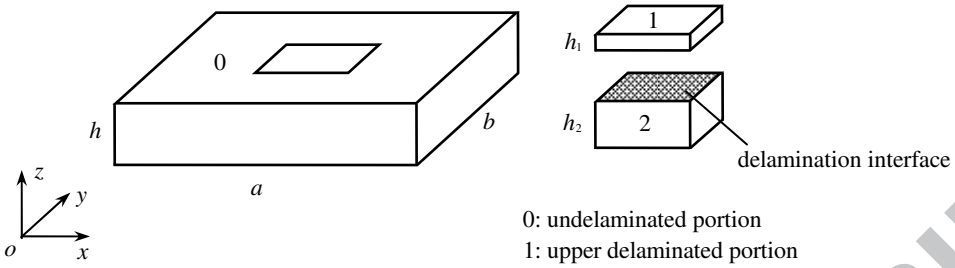

0: undelaminated portion
1: upper delaminated portion
2: lower delamianted portion

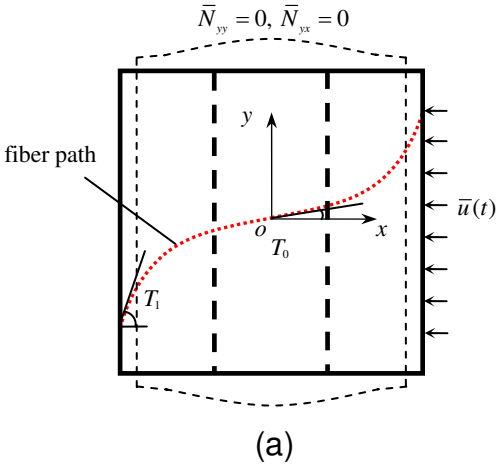

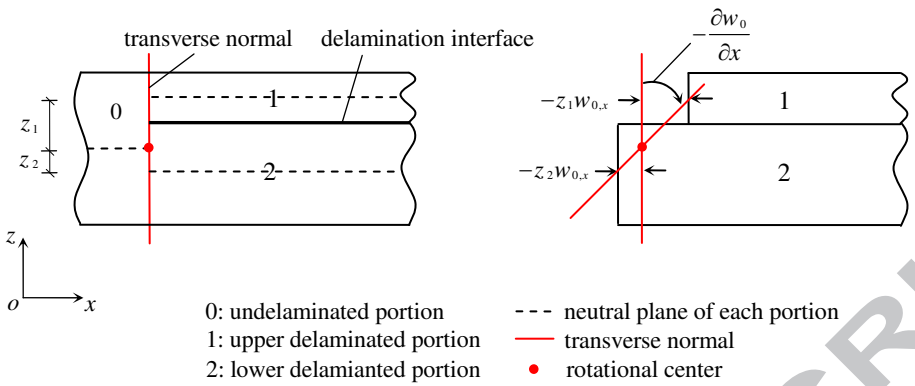

0: undelaminated portion
1: upper delaminated portion
2: lower delamianted portion

neutral plane of each portion
transverse normal
rotational center

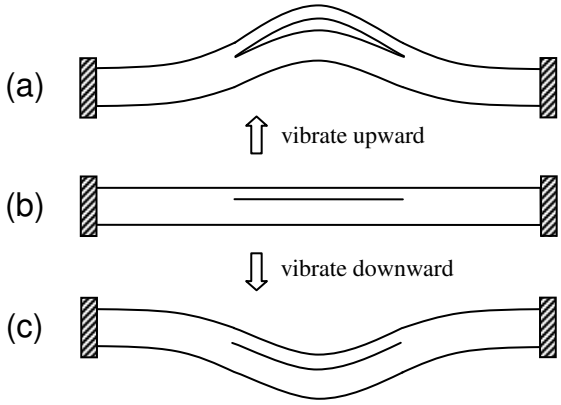

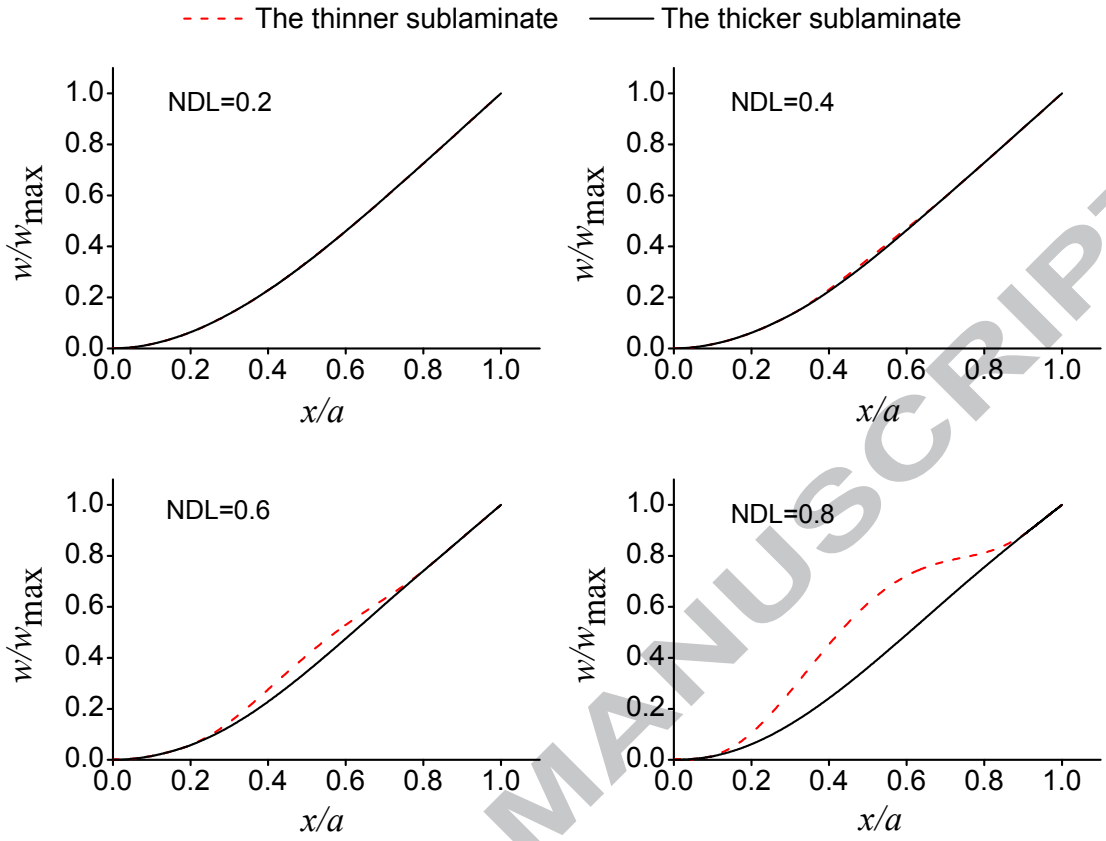

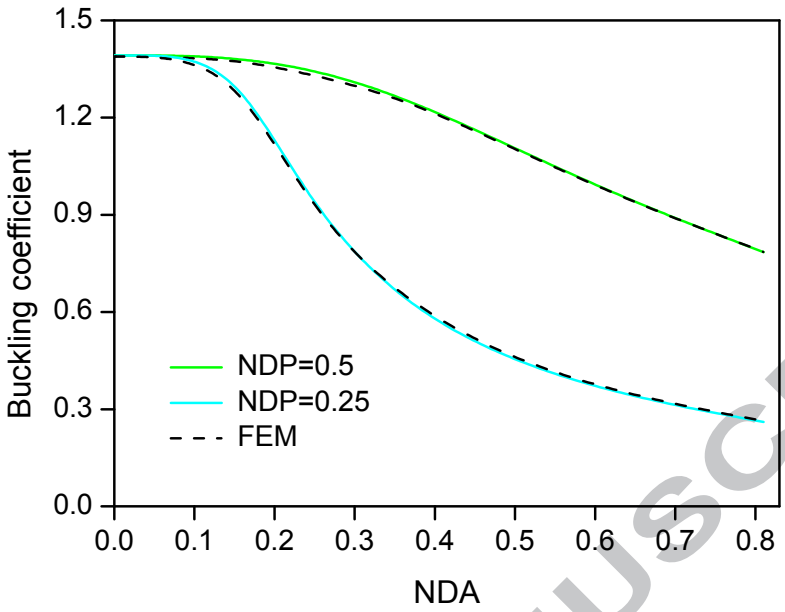

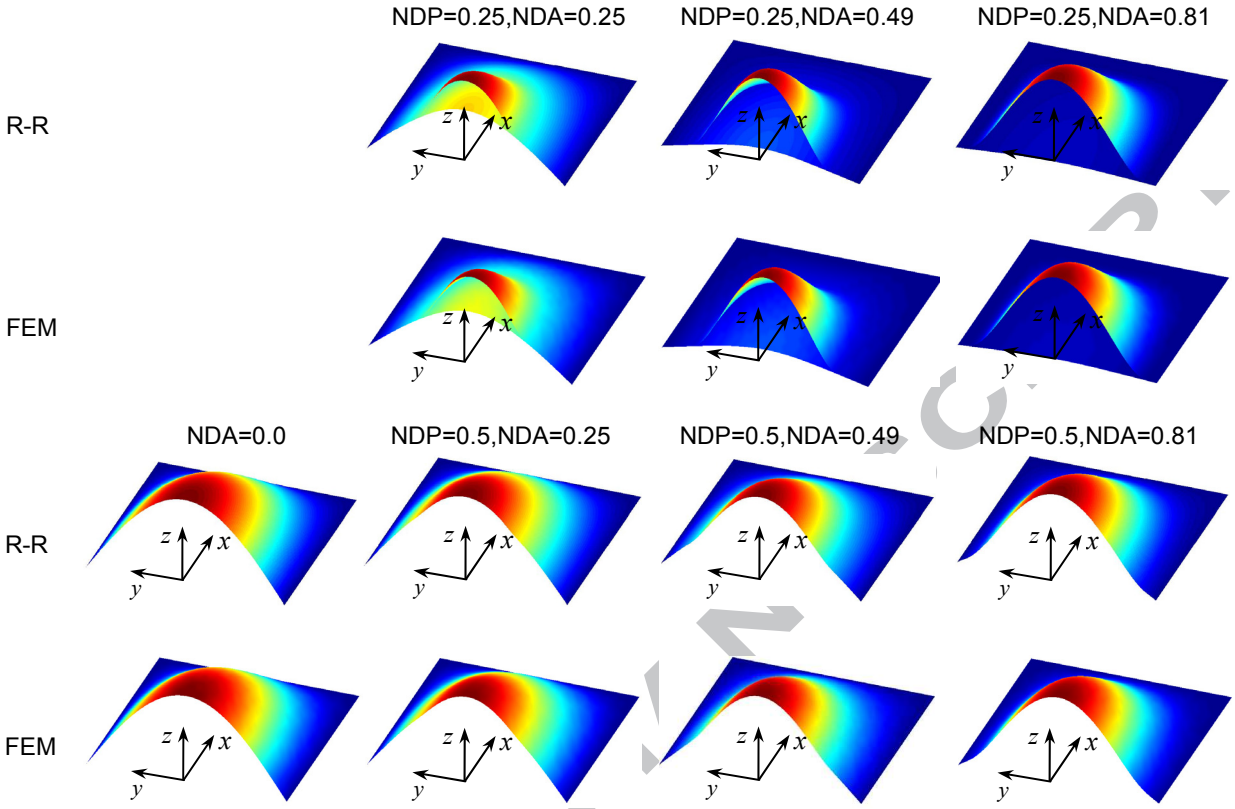

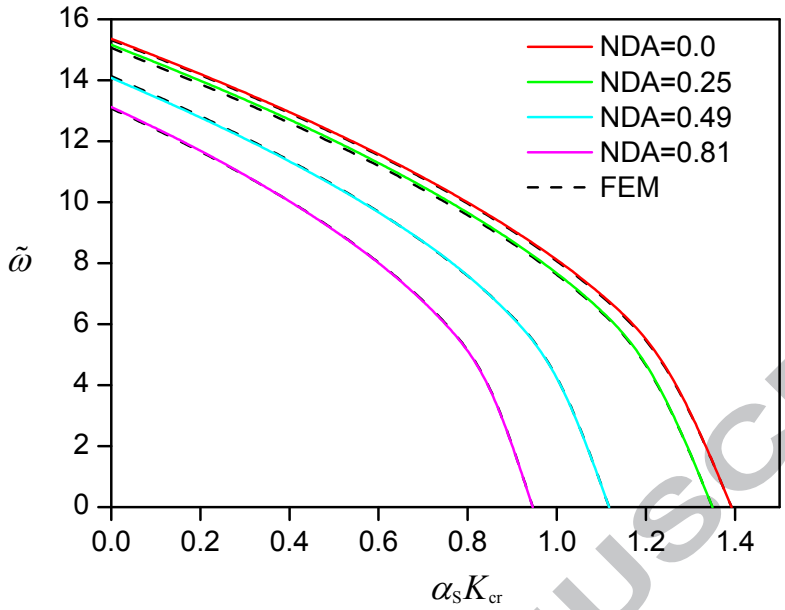

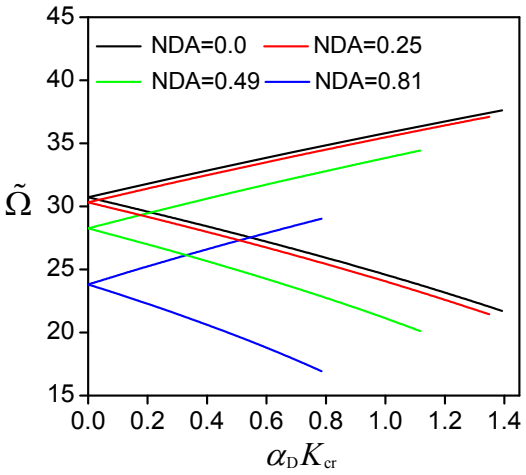

(a)

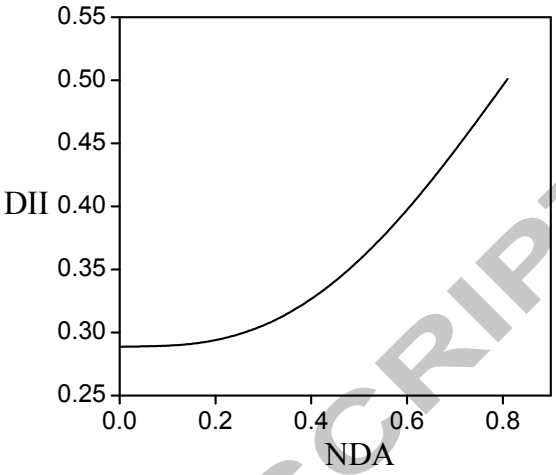

(b)

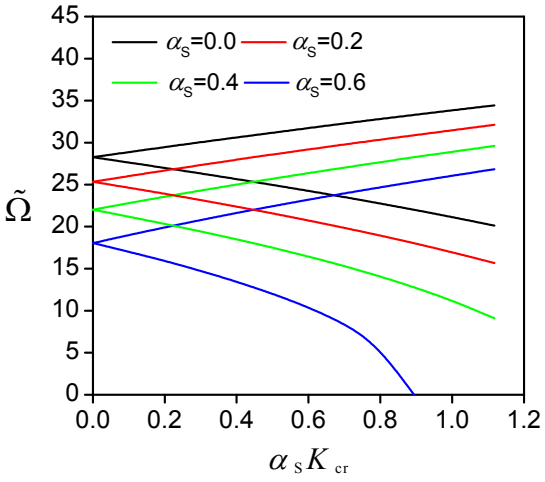

(a)

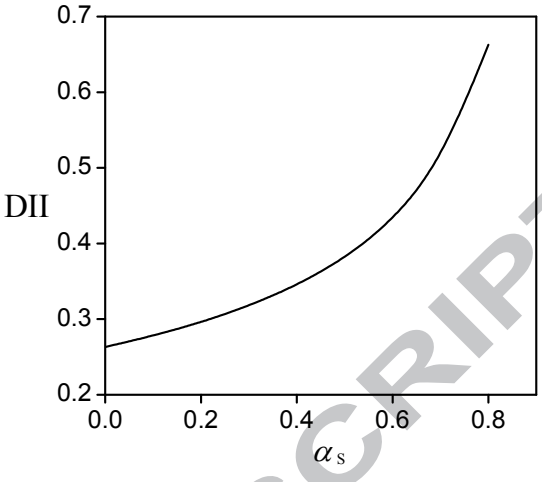

(b)